# Large eddy simulation of an ethylene–air turbulent premixed V-flame

Y.Y. Wu [a,b], C.K. Chan [a,*], L.X. Zhou [c]

[a] *Department of Applied Mathematics, The Hong Kong Polytechnic University, Hung Hom, Kowloon, Hong Kong*
[b] *Institute of Applied Mathematics and Computational Physics, Beijing, China*
[c] *Department of Engineering Mechanics, Tsinghua University, Beijing, China*

**A R T I C L E   I N F O**

**A B S T R A C T**

Large eddy simulation (LES) using a dynamic eddy viscosity subgrid scale stress model and a fast-chemistry combustion model without accounting for the finite-rate chemical kinetics is applied to study the ignition and propagation of a turbulent premixed V-flame. A progress variable $c$-equation is applied to describe the flame front propagation. The equations are solved two dimensionally by a projection-based fractional step method for low Mach number flows. The flow field with a stabilizing rod without reaction is first obtained as the initial field and ignition happens just upstream of the stabilizing rod. The shape of the flame is affected by the velocity field, and following the flame propagation, the vortices fade and move to locations along the flame front. The LES computed time-averaged velocity agrees well with data obtained from experiments.

© 2011 Elsevier B.V. All rights reserved.

## 1. Introduction

In practice, turbulent premixed combustion is considerably important. To investigate the interaction of turbulence with the flame front, a variety of simplified configurations have been studied experimentally: (1) turbulent V-flame, (2) swirl-stabilized flame, (3) Bunsen and stagnation flame. Numerical simulation of turbulent flame is a fast growing area but still remains a challenging task [1].

For turbulent flows, three basic approaches can be applied to do the simulations: (1) direct numerical simulation (DSN), (2) unsteady Reynolds averaging based numerical simulation (U-RANS) and (3) large eddy simulation (LES). DNS resolves all scale structures and velocity fluctuations, which are computationally expensive. U-RANS models the turbulence and only resolves unsteady mean flow structure, while model coefficients are often a problem for new configurations and also are frequently too dissipative. In the LES approach, the large-scale turbulence is solved whereas the small-scale turbulence is modeled. The simplest LES approach is to use no subgrid scales (SGS) [2]. In recent years, LES methods have many successful applications on turbulent combustion problems [3–8].

In this work, turbulent premixed V-flame has been studied numerically. A stabilized V-flame can be obtained by introducing a rod in a stream of fully premixed reactants. Chan et al. [9] studied the turbulent premixed V-flame without buoyancy with the discrete vortex method. Chan et al. [10] investigated the effect of intense turbulence on turbulent premixed V-flame. Bell et al. [11] simulated a laboratory-scale V-flame without a turbulence model, a burning velocity model, or any other type of turbulence closure hypothesis.

In the present work, the LES method with a dynamic model is used to simulate the propagation of a turbulent premixed V-flame. The flame front is followed by applying a progress variable equation. A projection-based fractional step method is applied to deal with velocity.

---

* Corresponding author. Tel.: +852 2766 6919; fax: +852 2334 4377.
  *E-mail address:* ck.chan@polyu.edu.hk (C.K. Chan).

The purpose of this paper is to study the interaction of the turbulence with the flame front. By numerical simulation, we presented the flame front propagation after ignition just upstream of the stabilizing rod. In addition, the vortex structure of the field is displayed with the flame front moving and the heat releasing.

## 2. Basic equations

For many applications relying on combustion, practical devices are operated at low flow speeds and very low Mach number. For typical premixed flame experiments, the fluid velocity is $U \approx$ 3–30 m/s while the speed of sound in the hot product gases is $c \approx$ 1000 m/s, an acoustic wave propagating at a speed $U + c$ [12]. Therefore the time scale of fluid motion is considerably longer than the time scale of the acoustic wave propagation. The fastest characteristic time scale is associated with the propagation of acoustic wave. Thus, an explicit time integration of control equations leads to severe time-step limitations corresponding to the most critical time scale. Using compressible equations for very low Mach number cases is then particularly inefficient. It is better to consider a low Mach number approximation. For low Mach cases, it is demonstrated that the low Mach number formulation is extremely efficient and the numerical simulation can keep a similar accuracy of direct numerical simulation for the flame properties [13].

Using non-dimensional parameters to analyze, the equations for reaction flows can be gained under the conditions of $Ma \ll 1$ and $p(\vec{x}, t) = p_0 + p'(\vec{x}, t)$ for an open domain. The simplified dimensionless control equations can be obtained as follows.

$$\frac{\partial \rho}{\partial t} + \frac{\partial (\rho u_j)}{\partial x_j} = 0 \tag{1}$$

$$\frac{\partial (\rho u_i)}{\partial t} + \frac{\partial (\rho u_i u_j)}{\partial x_j} = -\frac{\partial p'}{\partial x_i} + \frac{\partial \tau_{ij}}{\partial x_j} \tag{2}$$

$$\frac{\partial (\rho c)}{\partial t} + \frac{\partial (\rho u_j c)}{\partial x_j} = \rho S_d |\nabla c| \tag{3}$$

where $\rho$, $u$, $p'$, $c$, $t$ denote the density, velocity, pressure fluctuation, progress variable and time, respectively. $\tau_{ij} = \frac{\mu}{\text{Re}}(\frac{\partial u_i}{\partial x_j} + \frac{\partial u_j}{\partial x_i} - \frac{2}{3}\delta_{ij}\frac{\partial u_k}{\partial x_k})$ and $\mu$ is dynamic viscosity, Re is Reynolds number of the flow, and $\delta_{ij}$ is the Kronecker delta function.

To apply LES, the variables are filtered in physical space. The motions of large scales are explicitly solved from the filtered equations while the effects of cut-off scales motion are modeled. A filtered flow variables $\overline{\phi}$ is obtained by the applied filter function $F$ with filter width $\Delta$ to a flow variable $\phi$.

$$\overline{\phi}(x, t, \Delta) = \int_{-\infty}^{\infty} F(x - x'; \Delta)\phi(x', t)\mathrm{d}x'. \tag{4}$$

For variable density flows, a Favre filtering is introduced $\overline{\rho\phi} = \bar{\rho}\tilde{\phi}$. After the filtering operation, the filtered control equations are such as

$$\frac{\partial \bar{\rho}}{\partial t} + \frac{\partial (\bar{\rho}\tilde{u}_j)}{\partial x_j} = 0 \tag{5}$$

$$\frac{\partial (\bar{\rho}\tilde{u}_i)}{\partial t} + \frac{\partial (\bar{\rho}\tilde{u}_i\tilde{u}_j)}{\partial x_j} = -\frac{\partial p'}{\partial x_i} + \frac{\partial m_{ij}}{\partial x_j} \tag{6}$$

$$\frac{\partial (\bar{\rho}\tilde{c})}{\partial t} + \frac{\partial (\bar{\rho}\tilde{u}_j\tilde{c})}{\partial x_j} + \frac{\partial [\bar{\rho}(\widetilde{u_j c} - \tilde{u}_j\tilde{c})]}{\partial x_j} = \overline{\rho S_d |\nabla c|} = \rho_u S_L \Sigma \tag{7}$$

where $m_{ij} = \mu^+(\frac{\partial \tilde{u}_i}{\partial x_j} + \frac{\partial \tilde{u}_j}{\partial x_i} - \frac{2}{3}\delta_{ij}\frac{\partial \tilde{u}_k}{\partial x_k})$ and $\mu^+ = \mu_t + \mu/\text{Re}$, $\mu_t$ is the turbulent viscosity $\mu_t = \bar{\rho}C\Delta^2(2\tilde{S}_{kl}\tilde{S}_{kl})^{1/2}$ while $\tilde{S}_{kl}$ is the filtered strain rate tensor $\tilde{S}_{kl} = \frac{1}{2}(\frac{\partial \tilde{u}_k}{\partial x_l} + \frac{\partial \tilde{u}_l}{\partial x_k})$, and $C$ is the model constant, which is calculated using a dynamic model [14].

In the dynamic model, a second filter function is applied to the filtered momentum equation with filter width $\hat{\Delta}$ larger than $\Delta$. While the SGS stress tensor is $T_{ij} = \bar{\rho}\widetilde{u_i u_j} - \bar{\rho}\tilde{u}_i\tilde{u}_j$, a similar expression is achieved for the new sub-test scale (STS) stress tensor $\Gamma_{ij} = \widehat{\bar{\rho}\widetilde{u_i u_j}} - \widehat{\bar{\rho}\tilde{u}_i\tilde{u}_j}$. In the same way to define the SGS stress tensor, it can be modeled as:

$$\begin{cases} T_{ij} - \frac{1}{3}\delta_{ij}T_{kk} = -2C\bar{\rho}\Delta^2(2\widetilde{S}_{kl}\widetilde{S}_{kl})^{1/2}\widetilde{S}_{ij} = C\alpha_{ij} \\ \Gamma_{ij} - \frac{1}{3}\delta_{ij}\Gamma_{kk} = -2C\widehat{\bar{\rho}}\widehat{\Delta}^2(2\widehat{\widetilde{S}}_{kl}\widehat{\widetilde{S}}_{kl})^{1/2}\widehat{\widetilde{S}}_{ij} = C\beta_{ij}. \end{cases} \tag{8}$$

Define $L_{ij} = \widehat{\bar{\rho}\widetilde{u_i}\widetilde{u_i}} - \widehat{\bar{\rho}}\widehat{\widetilde{u_i}}\widehat{\widetilde{u_i}} = \Gamma_{ij} - \widehat{T}_{ij}$, then $C$ can be obtained from Eq. (8)

$$C = -\frac{L_{ij}(\widehat{\alpha}_{ij} - \beta_{ij})}{(\widehat{\alpha}_{kl} - \beta_{kl})(\widehat{\alpha}_{kl} - \beta_{kl})}. \tag{9}$$

In $c$-equation, the unclosed transport flux $\bar{\rho}(\widetilde{u_j c} - \widetilde{u_j}\widetilde{c})$ is modeled with a simple gradient expression $\bar{\rho}(\widetilde{u_j c} - \widetilde{u_j}\widetilde{c}) = -\frac{\mu_t}{Sc_t}\frac{\partial \tilde{c}}{\partial x_j}$. $\sum$ is the flame surface density, and is computed using a new model proposed in [15]. Based on the curvature of the filtered progress variable, the flame surface density is decomposed into a resolved and an unresolved contribution.

$$\Sigma = |\nabla \tilde{c}| + \kappa \overline{|\nabla \cdot N| M(\tilde{c})} \tag{10}$$

where $\kappa$ is a non-dimensional model parameter, $N = \nabla\tilde{c}/|\nabla\tilde{c}|$ is the unit vector normal to the iso-contours of the filtered progress variable and $M$ is a masking function to avoid undesired contributions in regions far away from the flame front.

## 3. Numerical methods

The structure of the control equations is similar to the constant density incompressible Navier–Stokes equations. For incompressible flows, projection-based fractional step methods have been proven to be an efficient discretization strategy. For low Mach number reaction flows, projection-based fractional step methods [13,16,4,17,18] and the generalized projection approach based on Helmholtz–Hodge decomposing theory [11,12] both have successful applications.

The projection-based fractional step method [13] is briefly described below. The basic idea is to solve the momentum equation in two consecutive parts. In the first step, it is integrated considering a constant pressure. Afterward, the pressure perturbation $p'(\vec{x}, t)$ is determined before performing the second integration step. And then the field velocities are corrected according to the pressure fluctuation gradient. The corresponding equations are:

$$\begin{cases} (\bar{\rho}\tilde{u}_i)^* = (\bar{\rho}\tilde{u}_i)^n + \Delta t \left[ -\frac{\partial(\bar{\rho}\tilde{u}_i\tilde{u}_j)}{\partial x_j} + \frac{\partial m_{ij}}{\partial x_j} \right] \\ (\bar{\rho}\tilde{u}_i)^{n+1} = (\bar{\rho}\tilde{u}_i)^* + \Delta t \left[ -\frac{\partial p'}{\partial x_i} \right]. \end{cases} \tag{11}$$

The pressure perturbation is determined by taking the divergence of the second equation above and introducing the continuity to estimate $\nabla \cdot (\rho\vec{u})^n$, leading to the following Poisson equation for $p'(\vec{x}, t)$:

$$\nabla^2 p' = \frac{1}{\Delta t}[(\partial_t \bar{\rho})^{n+1} + \nabla \cdot (\bar{\rho}\,\vec{u}\,)^*]. \tag{12}$$

The dilatation induced by heat release is taken into account through the introduction of the density variation term $(\partial_t \bar{\rho})^{n+1}$.

In the space discretization, the staggered grid is used and the finite difference method is applied to solve the control equations. In temporal discretization, the third order Runge–Kutta method is used in solving the velocity $\vec{u}$.

## 4. Simulation results and discussion

The numerical method discussed above is applied to simulate the premixed V-flame in turbulent flow field. The V-shaped flame is obtained by introducing a rod as a flame holder in a stream of premixed reactants. The computation conditions are according to the experiments of Cheng [19]. The schematic diagram of the experimental setup is shown in Fig. 1. The reactants studied are ethylene–air mixture ($C_2H_4$/air). The equivalence ratio of the mixture is 0.7 and the density ratio of reactants to products is $\rho_u/\rho_b = 6.7$. The mean inflow velocity is $U_0 = 5.5$ m/s, and the laminar flame speed is taken as $S_L = 0.35$ m/s. The reference length is defined as 50 mm from the diameter of the inner coaxial cylinder used in the experiments. The diameter of the rod as flame holder is 1 mm. The computational domain is $[-60 \text{ mm}, 60 \text{ mm}] \times [0, 120 \text{ mm}]$. All statistical results are obtained by averaging the instantaneous values over 8000 time steps.

The turbulent inflow is obtained by imposed velocity fluctuation on the mean value. Fig. 2 displays the fluctuation of the velocities at $y = 10$ mm, which is 10 mm upstream of the stabilizing rod. The turbulent intensity is about 7%.

The flow field with the stabilizing rod without reaction is first obtained as the initial field. The vorticity of the initial flow field is presented in Fig. 3, from which coherent large and strong vortex can be obviously observed downstream of the rod. The line and the dashed line respectively present positive and negative vorticities.

Fig. 4 shows the mean axial velocity downstream of the stabilizing rod at different locations. The velocity behind the rod is much less than the inflow velocity and around velocity. Closer to the flame holder, the axial velocity is smaller.

To study the interaction between the turbulent vortex and the flame front, flame front propagating after ignition happening upstream of the stabilizing rod is simulated. The process of propagation of the flame front is displayed in Fig. 5. The flame position is defined by the progress variable $\tilde{c} = 0.5$. From Fig. 5(a)–(c), the initial shape of the flame is largely affected by the velocity and the vortex behind the rod. The flow field behind the rod decides the stabilization and propagation
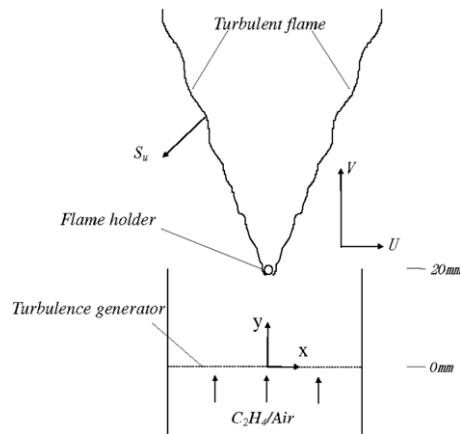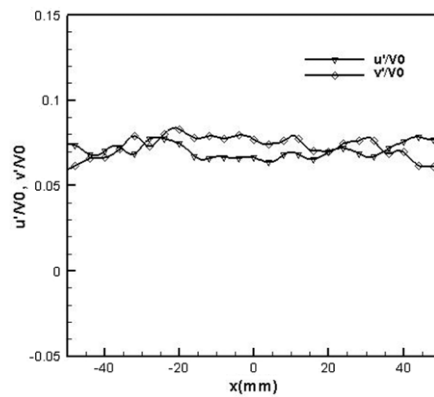
**Fig. 1.** Schematic diagram of a rod stabilized V-flame.



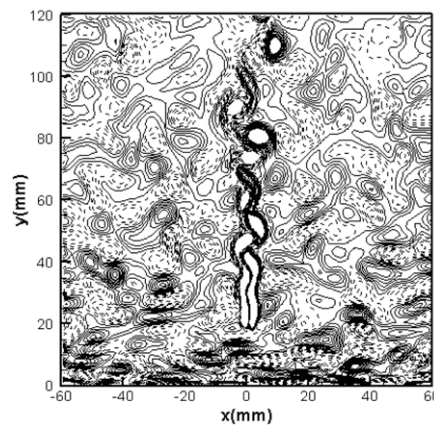**Fig. 2.** Fluctuation of the velocities at $y = 10$ mm.



**Fig. 3.** Vorticity of flow field stabilized by a rod without reaction.

of the flame front. At the beginning, the two wings of the flame propagate faster than the flame at the center. Then after the flame front reaches $y = 100$ mm, the flame at the center starts to propagate faster than the two wings of the flame.

With the flame front propagating and the heat releasing, the vortices fade in the burned field. In this process, the turbulence may be damped, which had been mentioned in [1] about the interaction of turbulence and combustion.

The computed instantaneous velocity and the flame position are shown in Fig. 6. The instantaneous flame front is wrinkled by the turbulence.
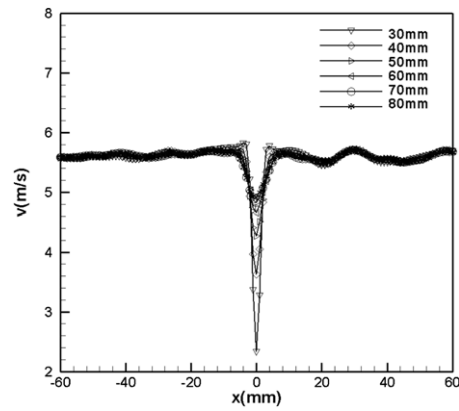
**Fig. 4.** Mean axial velocity without reaction.



(a) $T = 0.00045$ s.

(b) $T = 0.00227$ s.

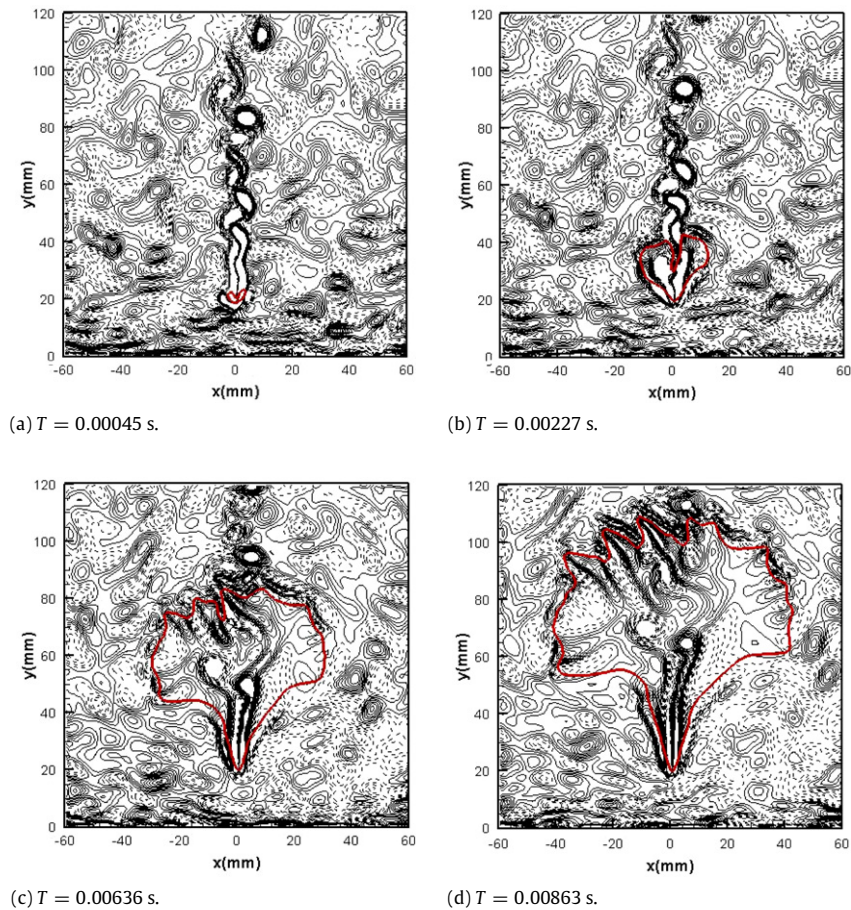(c) $T = 0.00636$ s.

(d) $T = 0.00863$ s.

**Fig. 5.** Flame front and vorticity change with time.

The computed mean velocity vector and mean flame position for turbulent inflow and for laminar inflow are compared in Fig. 7. The flame speed is increased by the flame wrinkling arising from turbulence. The reaction rate is increased by the flame wrinkling, which can be shown by the angle of the mean flame position.

The computed and measured transverse and axial velocity profiles are displayed at different $y$ positions in Figs. 8 and 9, respectively. According to the domain of computation and experiment [19], $y = 20$ mm in computation corresponds to $y = 50$ mm in experiment. The computed and measured velocity profiles are very similar. Comparing to the experimental data, the computed transverse velocities are little bigger outside the flame front and the maximal axial velocity is also bigger.
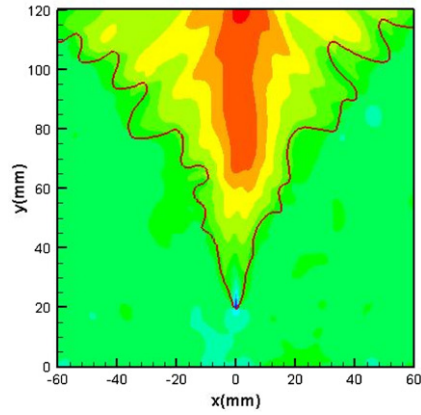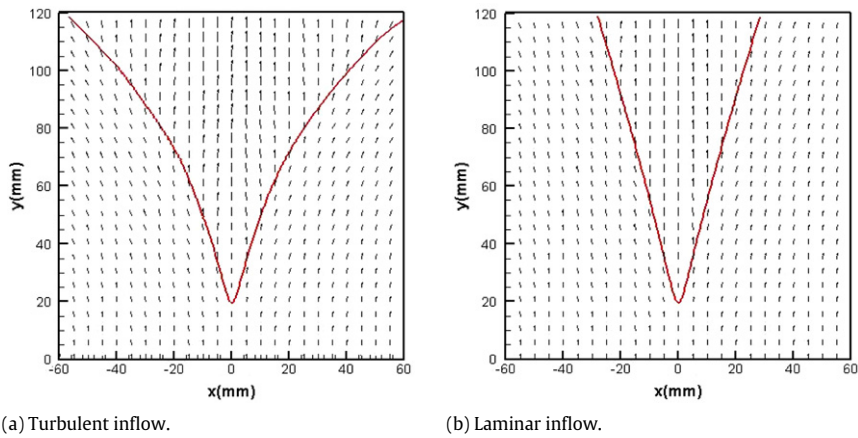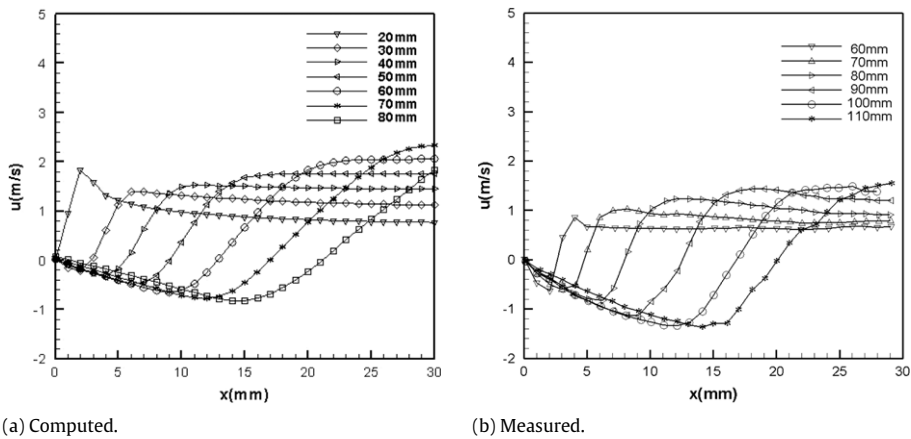
**Fig. 6.** Instantaneous velocity and flame front.



(a) Turbulent inflow.

(b) Laminar inflow.

**Fig. 7.** Mean velocity and mean flame position.



(a) Computed.

(b) Measured.

**Fig. 8.** Mean transverse velocity profiles at different *y* position.

The differences may be accounted for different inflow turbulent intensities and different coflow mixtures. In the experiment, the coflow is air while it is fuel/air mixture in the numerical simulation. In further research, the coflow air will be included.
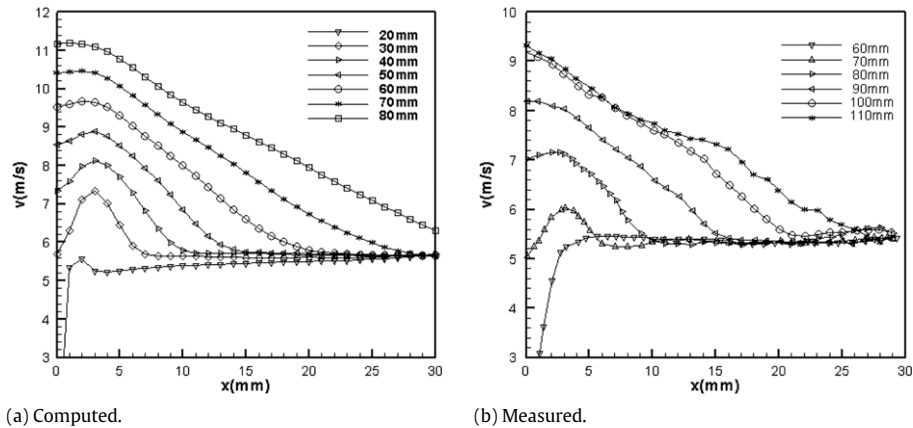
(a) Computed.　　　　　　　　　　　(b) Measured.

**Fig. 9.** Mean axial velocity profiles at different *y* position.

## 5. Conclusion

The propagation of a turbulent premixed V-flame is investigated by large eddy simulation with a dynamic model. The shape of the flame is determined by the velocity field and the vortex structure behind the stabilizing rod. The vortices fade in the burned field with the flame front propagating, which accompanies heat releasing. The larger angle of the mean flame position in turbulent flow field shows that the combustion rate is increased by the turbulence. These numerical simulation results display the interaction of flame front and turbulence. And the computed time-averaged velocities are comparable with the experimental data.

## Acknowledgements

## References

[1] T. Poinsot, D. Veynante, Theoretical and Numerical Combustion, 2001.
[2] J. Janicka, A. Sadiki, Large eddy simulation of turbulent combustion systems, Proceedings of the Combustion Institute 30 (2005) 537–547.
[3] M.P. Kirkpatrick, S.W. Armfield, A.R. Masri, S.S. Ibrahim, Large eddy simulation of a propagating turbulent premixed flame flow, Turbulence and Combustion 70 (2003) 1–19.
[4] Y. Liu, K.S. Lau, C.K. Chan, Y.C. Guo, W.Y. Lin, Structures of scalar transport in 2D transitional jet diffusion flames by LES, International Journal of Heat and Mass Transfer 46 (2003) 841–3851.
[5] V. Moureau, P. Minot, H. Pitsch, C. Bérat, A ghost-fluid method for large-eddy simulations of premixed combustion in complex geometries, Journal of Computational Physics 221 (2007) 600–614.
[6] A. Murrone, D. Scherrer, Large eddy simulation of a turbulent premixed flame stabilized by a backward facing step, in: 1st INCA Workshop, Villaroche, France, 2005.
[7] C. Nottin, R. Knikker, M. Boger, D. Veynante, Large eddy simulations of an acoustically excited turbulent premixed flame, Proceeding of the Combustion Institute 28 (2000) 67–73.
[8] P. Wang, X.S. Bai, Large eddy simulation of turbulent premixed flames using level-set *G*-equation, Proceedings of the Combustion Institute 30 (2005) 583–591.
[9] C.K. Chan, K.S. Lau, B.L. Zhang, Simulation of a premixed turbulent flame with the discrete vortex method, International Journal of Engineering Science 48 (2000) 613–627.
[10] C.K. Chan, H.Y. Wang, H.Y. Tang, Effect of intense turbulence on turbulent premixed V-flame, International Journal of Engineering Science 41 (2003) 903–916.
[11] J.B. Bell, M.S. Day, J.F. Grcar, M.J. Lijewski, M. Johnson, R.K. Cheng, I.G. Shepherd, Numerical simulation of a premixed turbulent V-flame, in: 19th International Colloquium on the Dynamics of Explosions and Reactive Systems, Japan, July, 2003.
[12] J.B. Bell, M.S. Day, J.F. Grcar, M.J. Lijewski, A computational study of equivalence ratio effects in turbulent, premixed methane–air flame, LBNL Report, LBNL-59246, in: Proc. ECCOMAS-CFD, 2006.
[13] J. de Charentenay, D. Thévennin, B. Zamuner, Comparision of direct numerical simulation of turbulent flames using compressible or low-Mach number formulations, International Journal for Numerical Methods in Fluids 39 (2002) 497–515.
[14] M. Germano, U. Poinmelli, P. Mooin, W.H. Cabot, A dynamic subgrid-scale eddy viscosity model, Physics of Fluids 3 (1991) 1760–1765.
[15] R. Knikker, D. Veynante, J.C. Rolon, C. Meneveau, Planar laser-induced fluorescence in a turbulent premixed flame to analyze large eddy simulation models, in: Proceedings of the 10th International Symposium on Turbulence, Heat and Mass Transfer, Lisbon, 2000.
[16] B. Lessani, M.V. Papalexandris, Time-accurate calculation of variable density flows with strong temperature gradients and combustion, Journal of Computational Physics 212 (2006) 218–246.
[17] H.N. Najm, P.S. Wyckoff, O.M. Knio, A semi-implicit numerical scheme for reacting flow: I. Stiff chemistry, Journal of Computational Physics 143 (1998) 381–402.
[18] F. Nicoud, Conservative high-order finite-difference schemes for low-Mach number flows, Journal of Computational Physics 158 (2000) 71–97.
[19] R.K. Cheng, Conditional sampling of turbulence intensities and Reynolds stress in premixed turbulent flames, Combustion Science and Technology 41 (1984) 109–142.